Noise-Immune Conjugate Large-Area Atom Interferometers

Sheng-wey Chiow,[1] Sven Herrmann,[1] Steven Chu,[1,2,3] and Holger Müller[1,2,3,*]

[1]*Physics Department, Stanford University, 382 Via Pueblo Mall, Stanford, California 94305, USA*
[2]*Department of Physics, University of California, 366 Le Conte Hall, Berkeley, California 94720-7300, USA*
[3]*Lawrence Berkeley National Laboratory, One Cyclotron Road, Berkeley, California 94720, USA*

(Received 13 January 2009; published 28 July 2009)

We present a pair of simultaneous conjugate Ramsey-Bordé atom interferometers using large ($20\hbar k$)-momentum transfer beam splitters, where $\hbar k$ is the photon momentum. Simultaneous operation allows for common-mode rejection of vibrational noise. This allows us to surpass the enclosed space-time area of previous interferometers with a splitting of $20\hbar k$ by a factor of 2500. Using a splitting of $10\hbar k$, we demonstrate a 3.4 ppb resolution in the measurement of the fine structure constant. Examples for applications in tests of fundamental laws of physics are given.

DOI: 10.1103/PhysRevLett.103.050402 PACS numbers: 03.75.Dg, 37.25.+k, 67.85.−d

Light-pulse atom interferometers can convert a small signal into a relatively large phase shift of the interference fringes. For example, in Ref. [1], a 3 ppb modulation in local gravity shifts the interference fringe by 1% of a cycle. They thus make excellent microscopes for small signals that have been applied in many cutting-edge precision measurements [1–10]. By using the momentum of many photons [11], rather than the two used in the above applications, the sensitivity of these interferometers can be increased by factors of tens or hundreds, by increasing the space-time area enclosed between the interferometer arms. But just as vibrations blur microscopic images, they blur the interference fringes in interferometers. This becomes more pronounced as the sensitivity is increased until eventually interferences can no longer be discerned. This has so far limited the use of large momentum transfer (LMT) beam splitters to very short pulse separation times T (Fig. 1) of 1 ms, thwarting the potential gain in sensitivity.

The effect of vibrations can be canceled between two interferometers that are addressed simultaneously by the same laser light [12–14]. In many applications, however, the configuration of the two interferometers needs to be different in order to produce the desired differential signal, and this can preclude the use of the same light to address them. More intricate beam splitting techniques will then be required to address both interferometers simultaneously.

In this work, we demonstrate such simultaneous conjugate interferometers (SCIs) and thereby unleash the potential of LMT in atom interferometers. Our SCIs are two Ramsey-Bordé interferometers; see Fig. 1. Each consists of four beam splitters which transfer momentum to one arm, separating it from the other arm and bringing it back. Conjugate interferometers are formed by using both outputs of the second beam splitter. In order to close both interferometers, the third and fourth beam splitters use laser pulses that contain a pair of frequencies. For interferometers with 20-photon momentum transfer [11], we demonstrate a 2500-fold increase in the enclosed space-time area, without a reduction in contrast. This paves the path towards strongly enhanced sensitivity in measurements of fundamental constants [8,9,15] or tests of general relativity [1]. Moreover, it will enable experiments which are impossible otherwise, such as cold-atom tests of the equivalence principle [10] and atom interferometric detection of gravitational waves [16].

Atom interferometers basically consist of a source of atoms and beam splitters for the matter waves. The atom source for our interferometers is a fountain of $\sim 10^6$ cesium atoms with a moving optical molasses launch and Raman sideband cooling in an optical lattice, as described in [17]. As beam splitters, we use multiphoton Bragg diffraction of matter waves at an optical lattice [11,18–20]. The optical lattice is formed by two counterpropagating laser beams that we may call the top and bottom beam (Fig. 2). Bragg diffraction can be described in the initial rest frame of the atom. For example, the atom may absorb n photons at ω_1 from the bottom beam and be stimulated to emit n photons at ω_2 into the top beam. The atom emerges at the same internal quantum state with a momentum of $2n\hbar k$, where k is the wave number, and a kinetic energy of $(2n\hbar k)^2/(2M)$,

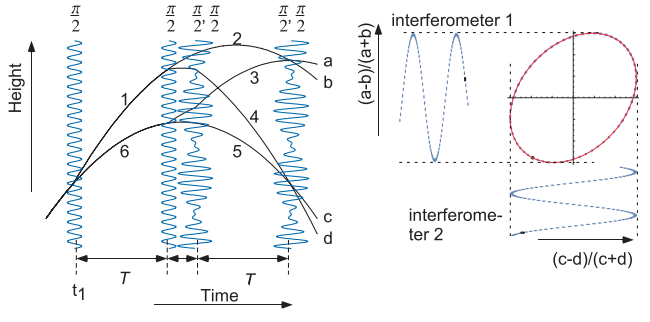

FIG. 1 (color online). Plotting the fringes of two interferometers against each other creates an ellipse, whose eccentricity allows one to determine the relative phase.

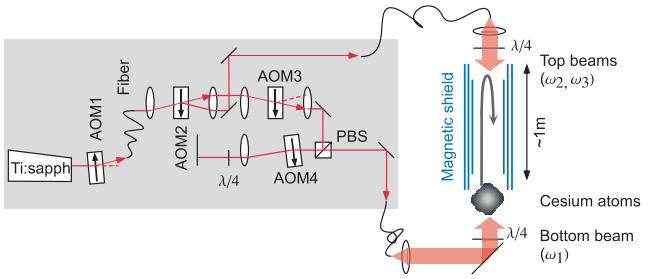

FIG. 2 (color online). Setup (simplified). Ti:sapph, Ti:sapphire laser; $\lambda/4$, retardation plate; PBS, polarizing beam splitter.

where M is the mass of the atom. This energy has to match the energy $n\hbar(\omega_1 - \omega_2)$ lost by the laser field, which allows us to choose the Bragg diffraction order n by the difference frequency $\omega_1 - \omega_2$.

Figure 1 (left) shows a space-time diagram of our Ramsey-Bordé interferometers. Let us specialize to the lower one, whose outputs are labeled (c) and (d). An atom enters on its way upwards. At a time t_1, a "$\pi/2$" laser pulse transfers a momentum of $2n\hbar k$ with a probability of 50%. Depending on whether momentum was transferred or not, the atom follows trajectory 1 or 6. At $t_1 + T$, a second $\pi/2$ pulse stops the relative motion of them. After two more pulses, the paths are recombined into the outputs (c) and (d) where they interfere. A second, upper, interferometer is formed by recombining the other outputs of the second beam splitter (at $t_1 + T$).

The probability that the atom arrives at output (c), for example, is given by $\cos^2\phi$, where $\phi = \phi_F + \phi_I$ is the phase difference of the interferometer arms when they interfere. This contains a contribution ϕ_F of the atom's free evolution between the beam splitters and one of the interaction with the light ϕ_I. The free evolution phase $\phi_F = S_{\mathrm{cl}}/\hbar$ is given by the classical action $S_{\mathrm{cl}} = \int(E_{\mathrm{kin}} - E_{\mathrm{pot}})dt$, where E_{kin} and E_{pot} are the kinetic and potential energy. The interaction phase ϕ_I is because whenever a photon is absorbed, its phase is added to the matter wave phase and subtracted for emission of a photon [21]. This phase is different for the two paths because of the respective spatial separation of the interactions at t_2 and t_3. Summing up, [8,11]

$$\phi^{\pm} = \pm 8n^2\omega_r T + 2nkg(T + T')T + n\phi_L^{\pm}, \qquad (1)$$

where $\omega_r = \hbar k^2/(2M)$ is the recoil frequency and g the local gravitational acceleration. The plus and minus signs are for the upper and lower interferometer, respectively, and $\phi_L^{\pm} = \phi_2 - \phi_1 - \phi_4^{\pm} + \phi_3^{\pm}$ is given by the phases ϕ_{1-4} of the laser pulses at t_{1-4}. Equation (1) shows that LMT beam splitters can increase the sensitivity of the phase towards gravity by a factor of n and the one towards the recoil by n^2.

Because of the motion of the atoms, which gives rise to a Doppler frequency shift, addressing the upper and lower interferometer requires two separate laser frequencies ω_2, ω_3 in the top beam. The phases of these respective frequencies are denoted $\phi_3^{\pm}$ and $\phi_4^{\pm}$.

As the atoms define an inertial frame, any vibrations of the laboratory translate into phase shifts of the laser beams in this frame. If the distribution of ϕ_L has a width larger than $\sim\pi/n$, the visibility V of the interferences (as defined by the amplitude of a sine wave fit) goes to zero. With non-LMT beam splitters, vibrations can be suppressed to acceptable levels by state-of-the-art vibration isolation [22]. This becomes difficult, however, with $n \gg 1$ LMT beam splitters.

The idea underlying the cancellation of vibrations is to run the upper and lower interferometers simultaneously (SCIs) and to use

$$\Phi \equiv \phi^+ - \phi^- = 16n^2\omega_r T + n\phi_L \qquad (2)$$

as an experimental observable, where $\phi_L = (\phi_3^+ - \phi_3^-) + (\phi_4^- - \phi_4^+)$ depends only upon the difference between laser phases at the last two beam splitters. Thus, the requirement of *absolute* phase stability in one individual interferometer has been reduced to one of *relative* stability between two: If this is the case, ϕ_L will remain constant even if the individual ϕ_{1-4} fluctuate strongly. Then, their fringes as plotted in Fig. 1 form an ellipse. The common phase moves the data points around the ellipse, but the differential phase can be extracted by ellipse-specific fitting even if the visibility $V = 0$ for the individual interferometers.

One essential requirement for the experimental setup (Fig. 2) is to satisfy $\delta\phi_L = 0$ as well as technically possible. Moreover, our laser system is optimized for driving LMT beam splitters based on high-order Bragg diffraction [11,20], which requires laser pulses having smooth envelope functions with an optimized duration and high power. The laser light originates from a 6 W injection-locked Ti:sapphire laser at 852 nm wavelength [11,23]. Its frequency is referenced to the Cs $F = 3 \rightarrow F' = 2$ $D2$ transition; an offset of up to ± 20 GHz can be set by means of an offset lock. For intensity control and forming the Gaussian envelope functions of the beam splitting pulses, we use an acousto-optical modulator AOM1 within a feedback loop.

As a result of the different motion of atoms in the two interferometers, the resonance conditions for the third and fourth beam splitter differ by $16n\omega_r$ between interferometers. To satisfy both, AOM2 is driven by two rf signals of equal amplitude at frequencies of 180 MHz $\pm f_m$. It thus generates two optical frequencies in its deflected output that differ by $2f_m$. They follow the same optical path; thus, phase fluctuations that may be caused, for example, by vibrations, air currents, etc., are common-mode, and do not degrade the phase noise in the difference frequency. We have previously shown that a phase variance of $\sigma^2 \approx (160\ \mu\mathrm{rad})^2$ can be achieved [24]. The power in each component is set to 1/8 of the power at the input of

AOM2, which maximizes the Rabi frequency of driving the atoms.

To generate the counterpropagating beam, we use the undeflected power from AOM2. This, however, varies between 1/2 and 1 of AOM2's input power at the beat frequency $2f_m$ of the two rf signals. AOM3 is used to take out this undesired modulation. It is driven by a "conjugate" rf signal, which is strong when the rf drive of AOM2 is weak and vice versa. The amplitude modulation is thus suppressed—residual sidebands are below 0.0018 (or −27 dB) of the carrier power.

Because of the free fall of the atoms, the resonance condition in the laboratory frame changes at a rate of about 23 MHz/s. We account for this by ramping the frequency of the bottom beam using the double-passed AOM4.

The beams are brought to the experiment via polarization-maintaining fibers and collimated to a $1/e^2$ radius w_0 of about 3 mm by a commercial fiber port (Thorlabs) or 12.5 mm by a triplet lens, a combination of an aplanatic meniscus (CVI Melles Griot 01 LAM 225/076) and an achromatic doublet (Thorlabs AC508-200B). The polarizations are made circular to $(\sigma^+ - \sigma^+)$ by zeroth-order quarter wave plates. The bottom beam can have a maximum power of 1.15 W at the fiber output, the top beam a peak power of 1.6 W, i.e., 0.4 W per frequency.

The first interferometer pulse typically starts at $t_1 =$ 70 ms after launch. For $20\hbar k$ beam splitters, we use a red detuning of about 3–4 GHz (relative to the $D2$ $F = 3 \rightarrow F' = 4$ line) and peak intensities of 0.4 W/cm^2 in the bottom beam and 0.13 W/cm^2 per frequency in the top beam with $w_0 = 12.5$ mm; with $w_0 = 3$ mm a detuning of 16 GHz is used. After elapse of the full interferometer sequence, the atoms in the four interferometer outputs a–d (Fig. 2, left) are separately detected by their fluorescence f_{a-d} as they pass a photomultiplier tube in free fall. To take out fluctuations in the atom number, we define the normalized fluorescence $F_u = (f_a - f_b)/(f_a + f_b)$ of the upper interferometer and F_l in analogy for the lower interferometer.

Figure 3 shows examples for ellipses measured by our SCIs at a short pulse separation time of $T = 1$ ms. A contrast (defined as the semimajor axis of the ellipse) of 25%–32% is achieved at momentum transfers between (8–20)$\hbar k$ (the theoretical optimum is 50%, because each detected interferometer output overlaps spatially with population lost in the third beam splitter which does not interfere). It is evident that the strong reduction in visibility at high momentum transfer, that was observed in previous LMT interferometers [11], is absent in the contrast of our SCIs.

The dependence of the contrast on the pulse separation time T is shown for $10\hbar k$ and $20\hbar k$ interferometers in Fig. 4 (left). The reduction of contrast for long pulse separation times has several reasons: (i) Thermal motion of the atoms causes them to leave the center of the Bragg beam, reducing the number of atoms that take part in the interference as T is increased; (ii) the same motion means different atoms sample the phase of the Bragg beams at different points. Uneven wave fronts of these beams thus cause a phase variation between the atoms, smearing out the interferences. To reduce this effect, we minimize the number of optical elements in the beams after the fibers (Fig. 2) and shield the beams from air currents. In addition, a retroreflection geometry was tested: the beams after AOM 3 and 4 are sent through the same fiber with orthogonal polarizations and the upper fiber collimation optics is replaced by a retroreflector and a quarter wave plate. This method led to the improved contrast for $\Delta p = 10\hbar k$, $T =$ 100 ms. In addition, it simplifies beam alignment. A contrast of 21% is obtained for $T = 100$ ms and $10\hbar k$. For a $20\hbar k$ interferometer, contrast is 10% at $T = 50$ ms. In previous work without SCIs, 8% visibility at $20\hbar k$ was only possible at $T \leq 1$ ms [11]. Thus, SCIs allow us to improve the pulse separation time to 50 ms from 1 ms, without a reduction in contrast. This corresponds to a 50-fold increase in the sensitivity of Ramsey-Bordé interferometers, see Eq. (2), and a 2500-fold increase in the enclosed space-time area.

The differential signal of our SCIs is the $16n^2\omega_r T$ term allowing for high-resolution measurements of the recoil frequency ω_r. To demonstrate this, Fig. 4 shows 1300 data points taken with a $T = 100$ ms, $10\hbar k$ interferometer pair. To analyze the data, we use a Bayesian estimation, which shows a better immunity from systematic errors than simpler methods [25]; see Ref. [13]. From a total of 12 000 such points, we obtain a resolution of 6.8 ppb within 7 h of

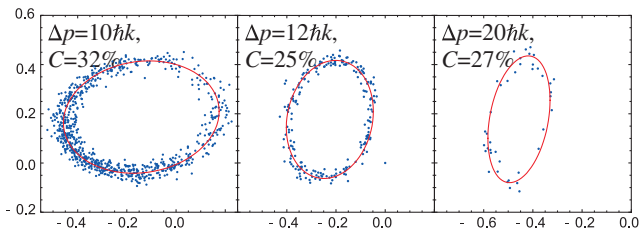

FIG. 3 (color online). Experimental ellipses obtained by plotting the normalized fluorescence F_u, F_l of an SCI pair against each other. $T = 2$ ms. An uneven distribution of data may result at such short T, if the common-mode phase is not fully randomized.

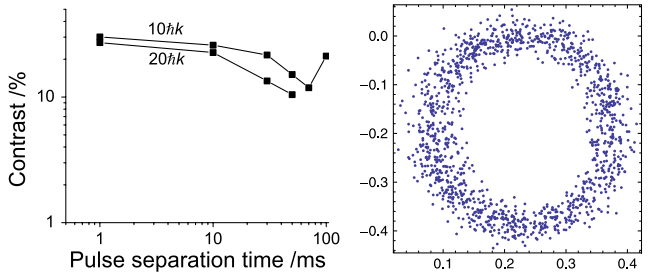

FIG. 4 (color online). Left: Contrast versus pulse separation time for $10\hbar k$ and $20\hbar k$ interferometers. Right: 1300 data points ($\Delta p = 10\hbar k$, $T = 100$ ms, $C = 20\%$).

measurement. Via Eq. (2), ω_r and thus $\hbar/M$ can be determined; correspondingly, our SCIs are sensitive to the fine structure constant α via $\alpha = [(2R_\infty/c)(M/m_e)(h/M)]^{1/2}$, where R_∞ is the Rydberg constant and m_e the electron mass, to a resolution of 3.4 ppb. Without SCIs and LMT, achieving a similar resolution would take several weeks' worth of data [8]. Our resolution compares favorably to previous work, which used $\sim 2000\hbar k$ common-mode momentum transfer. This previous work yields 3 ppb resolution in α, using 88 h of data [9]. Our improvement is because of (i) the n^2 scaling of the sensitivity with momentum transfer in our method, and (ii) cancellation of vibrational noise between SCIs. Further reduction of this statistical uncertainty and an analysis of systematic errors are beyond the scope of this Letter.

In the future, we will reduce wave front distortions with a mode-filtering cavity and should thus be able to reach $T = 500$ ms at $\Delta p = 20\hbar k$. The sensitivity, which is proportional to $(\Delta p)^2 T$, should then increase 20 times. Furthermore, an improved two-dimensional magneto-optical trap should increase the atom flux about tenfold. Also, our fluorescence detection now operates a factor of ~ 50 above the atom shot noise limit. Improved light collection optics should alleviate this.

With LMT, cancellation of vibrations will become vital in Mach-Zehnder interferometers (MZIs) as well. For example, vibration cancellation and LMT as demonstrated here is a crucial technology for atomic gravitational wave interferometric sensors [16]. Our work demonstrates that this is possible, opening up new perspectives in precision measurements: Many MZI applications gain sensitivity proportional to the enclosed area, which means that our work allows for a 2500-fold improvement compared to previous $20\hbar k$ interferometers.

Our methods can be extended to interferometers using different atomic species, or even different laser wave numbers k_1 and k_2. In the latter case, the phase relationship between these lasers could be established by a frequency comb. Cancellation of vibrations then requires that $k_1 n_1$ and $k_2 n_2$, where $n_{1,2}$ are the Bragg diffraction orders, satisfy a simple rational relationship. A Lissajous figure will then be generated which reduces to an ellipse for $k_1 n_1 = k_2 n_2$. Bayesian estimation can be used to extract the phase. The possibility of correlating signals from different atoms is interesting for tests of the equivalence principle [10,26], and may allow new paths to cancel systematic effects in searches for an electron electric dipole moment [27], tests of charge neutrality [28], and other experiments.

In this work, we have presented common-mode rejection between simultaneous conjugate atom interferometers addressed by different overlapped laser frequencies. Compared to previous work [11], we demonstrate a 2500-fold increase in the enclosed space-time area of atom interferometers using $20\hbar k$ momentum transfer, without a reduction in interference contrast. By removing the most important limitation on the space-time area, and hence sensitivity, of such large momentum transfer interferometers, this work opens the door towards many exciting experiments.

S. H. and H. M. thank the Alexander von Humboldt foundation. This material is based upon work supported by the National Science Foundation under Grant No. 0400866 and by the Air Force Office of Scientific Research under Grant Number FA9550-04-1-0040.

*hm@berkeley.edu; http://physics.berkeley.edu/research/mueller/

[1] H. Müller *et al.*, Phys. Rev. Lett. **100**, 031101 (2008); K.-Y. Chung *et al.*, Phys. Rev. D **80**, 016002 (2009).
[2] A. Peters, K. Y. Chung, and S. Chu, Nature (London) **400**, 849 (1999); Metrologia **38**, 25 (2001).
[3] T. L. Gustavson, A. Landragin, and M. A. Kasevich, Classical Quantum Gravity **17**, 2385 (2000).
[4] D. S. Durfee, Y. K. Shaham, and M. A. Kasevich, Phys. Rev. Lett. **97**, 240801 (2006).
[5] B. Canuel *et al.*, Phys. Rev. Lett. **97**, 010402 (2006).
[6] J. B. Fixler *et al.*, Science **315**, 74 (2007).
[7] G. Lamporesi *et al.*,Phys. Rev. Lett. **100**, 050801 (2008).
[8] A. Wicht *et al.*, Phys. Scr. **T102**, 82 (2002).
[9] P. Cladé *et al.*, Phys. Rev. Lett. **96**, 033001 (2006); Phys. Rev. A **74**, 052109 (2006); M. Cadoret *et al.*, Phys. Rev. Lett. **101**, 230801 (2008).
[10] S. Dimopoulos *et al.*, Phys. Rev. Lett. **98**, 111102 (2007); Phys. Rev. D **78**, 042003 (2008).
[11] H. Müller *et al.*, Phys. Rev. Lett. **100**, 180405 (2008).
[12] M. J. Snadden *et al.*, Phys. Rev. Lett. **81**, 971 (1998).
[13] J. K. Stockton, X. Wu, and M. A. Kasevich, Phys. Rev. A **76**, 033613 (2007).
[14] A. Bertoldi *et al.*, Eur. Phys. J. D **40**, 271 (2006).
[15] H. Müller *et al.*, Appl. Phys. B **84**, 633 (2006).
[16] S. Dimopoulos *et al.*, Phys. Rev. D **78**, 122002 (2008); Phys. Lett. B **678**, 37 (2009).
[17] P. Treutlein, K. Y. Chung, and S. Chu, Phys. Rev. A **63**, 051401(R) (2001).
[18] D. M. Giltner, R. W. McGowan, and S. A. Lee, Phys. Rev. Lett. **75**, 2638 (1995); Phys. Rev. A **52**, 3966 (1995).
[19] A. Miffre *et al.*, Eur. Phys. J. D **33**, 99 (2005).
[20] H. Müller, S.-w. Chiow, and S. Chu, Phys. Rev. A **77**, 023609 (2008).
[21] D. S. Weiss, B. C. Young, and S. Chu, Appl. Phys. B **59**, 217 (1994).
[22] J. M. Hensley, A. Peters, and S. Chu, Rev. Sci. Instrum. **70**, 2735 (1999).
[23] S.-w. Chiow *et al.*, Opt. Express **17**, 5246 (2009).
[24] H. Müller *et al.*, Opt. Lett. **31**, 202 (2006).
[25] G. T. Foster *et al.*, Opt. Lett. **27**, 951 (2002).
[26] W. Ertmer *et al.*, Exp. Astron. **23**, 611 (2009).
[27] C. Chin *et al.*, Phys. Rev. A **63**, 033401 (2001).
[28] M. Kasevich and S. Chu, Phys. Rev. Lett. **67**, 181 (1991); C. Lämmerzahl, A. Macias, and H. Müller, Phys. Rev. A **75**, 052104 (2007); A. Arvanitaki *et al.*, Phys. Rev. Lett. **100**, 120407 (2008).